JOURNAL OF GEOPHYSICAL RESEARCH, VOL. 106 , NO. D15, PAGES 17,221–17,235, AUGUST 16, 2001

Direct observations of clear-sky aerosol radiative forcing from space during the Indian Ocean Experiment

K. Rajeev[1]
Space Physics Laboratory, Vikram Sarabhai Space Centre, Trivandrum, India

V. Ramanathan
Center for Clouds, Chemistry and Climate, Scripps Institution of Oceanography, University of California, San Diego, La Jolla, California

Abstract. This study presents the regional estimates of the seasonal and diurnal mean broadband (0.3–5.0 μm) clear-sky aerosol radiative forcing at the top of atmosphere (TOA) due to both the natural and the anthropogenic aerosols over the tropical Indian Ocean from 25°N to 25°S. We propose two new methods, the slope method and the differencing method, to obtain clear sky aerosol forcing from solely satellite measurements. The focus of the study is January to March 1997, 1998, and 1999. The TOA clear-sky aerosol forcing was obtained by integrating satellite data for aerosol optical depth (AOD) and the broadband radiation budget. Over 30,000 pixels were collocated to estimate that the diurnal and seasonal mean reflected broadband solar radiation at TOA increases by about 24 W m^{-2} per unit increase in AOD at the wavelength of 500 nm. The observed TOA clear-sky aerosol forcing varied between -4 and -14 W m^{-2} in the Northern Hemisphere (NH) and between 0 and -6 Wm^{-2} in the Southern Hemisphere. Assuming a ratio of surface to TOA clear-sky aerosol forcing of 3 which was observed over Kaashidhoo Climate Observatory (4.96°N, 73.46°E) during the same period [*Satheesh and Ramanathan*, 2000], this leads to a clear-sky aerosol forcing of -12 to -42 Wm^{-2} at the surface in the NH. The difference between the TOA forcing and the surface forcing is the atmospheric forcing. As a result, the atmosphere is subject to a large net forcing of about 8–28 Wm^{-2} in the NH, largely due to the presence of black carbon. Of equal importance is the fact that the Indian Ocean aerosols introduce a large interhemispheric gradient in the solar heating during the wintertime. The implications for climate and monsoonal circulation may be major and need to be explored with coupled model studies.

1. Introduction

Aerosols affect the radiation budget of Earth-atmosphere system by scattering and absorbing part of the incoming solar radiation (direct effect) and by modifying the cloud droplet size distribution, thereby changing the radiative properties and lifetime of clouds (indirect effect) [*Charlson et al.*, 1992; *Kiehl and Briegleb*, 1993; *Intergovernmental Panel on Climate Change (IPCC)*, 1995]. Both the direct and the indirect radiative effects of aerosols have large regional variations because of the short lifetime of aerosols, which contribute to significant spatial variability in aerosol concentrations as well as in their chemical composition and optical properties. A detailed investigation of aerosol radiative properties and the radiative forcing on a regional scale is thus essential. Such regional studies were carried out in the Amazon region [*Kaufman et al.*, 1998], in the western Atlantic Ocean [*Russell et al.*, 1999], and in the Indian Ocean [*Ramanathan et al.*, 1995]. The Tropospheric Aerosol Radiative Forcing Observational Experiment (TARFOX) made extensive measurements of aerosol properties and the radiative effects of aerosols in the summer haze plume of the east coast of the United States [*Russell et al.*, 1999] which showed that the instantaneous sky daytime upwelling flux changes due to aerosols are about 30–100 times larger than the global average forcing expected for a global average sulfate aerosol optical depth of 0.04 [*Hignett et al.*, 1999].

The Indian Ocean Experiment (INDOEX) was aimed at studying the long range transport of aerosols and trace species into the otherwise pristine oceans from urban regions and assessing the direct and the indirect aerosol radiative forcing [*Ramanathan et al.*, 1995]. During the Asian winter monsoon period, the northeasterly winds from the land areas transport large amounts of continental aerosols over the oceanic regions [*Rajeev et al.*, 2000]. This provides a unique opportunity to study the extent of transport of continental aerosols and their radiative impact over the otherwise pristine ocean areas. *Jayaraman et al.* [1998] studied the direct aerosol radiative forcing at Earth's surface over the tropical Indian Ocean on the basis of surface measurements of column aerosol optical depth and the incoming direct and diffuse solar radiation in the visible spectrum. They showed that the direct visible (<780 nm) solar flux decreased by 42 $\pm$ 4 Wm^{-2} and diffuse sky radiation increased by about 30 $\pm$ 3 Wm^{-2} with every 0.1 increase in aerosol optical depth for solar zenith angles smaller than 60°. By integrating the aerosol chemical and optical prop-

[1]Formerly at Center for Clouds, Chemistry, and Climate, Scripps Institution of Oceanography, University of California, San Diego, California.

Paper number 2000JD900723
0148-0227/01/2000JD900723$09.00

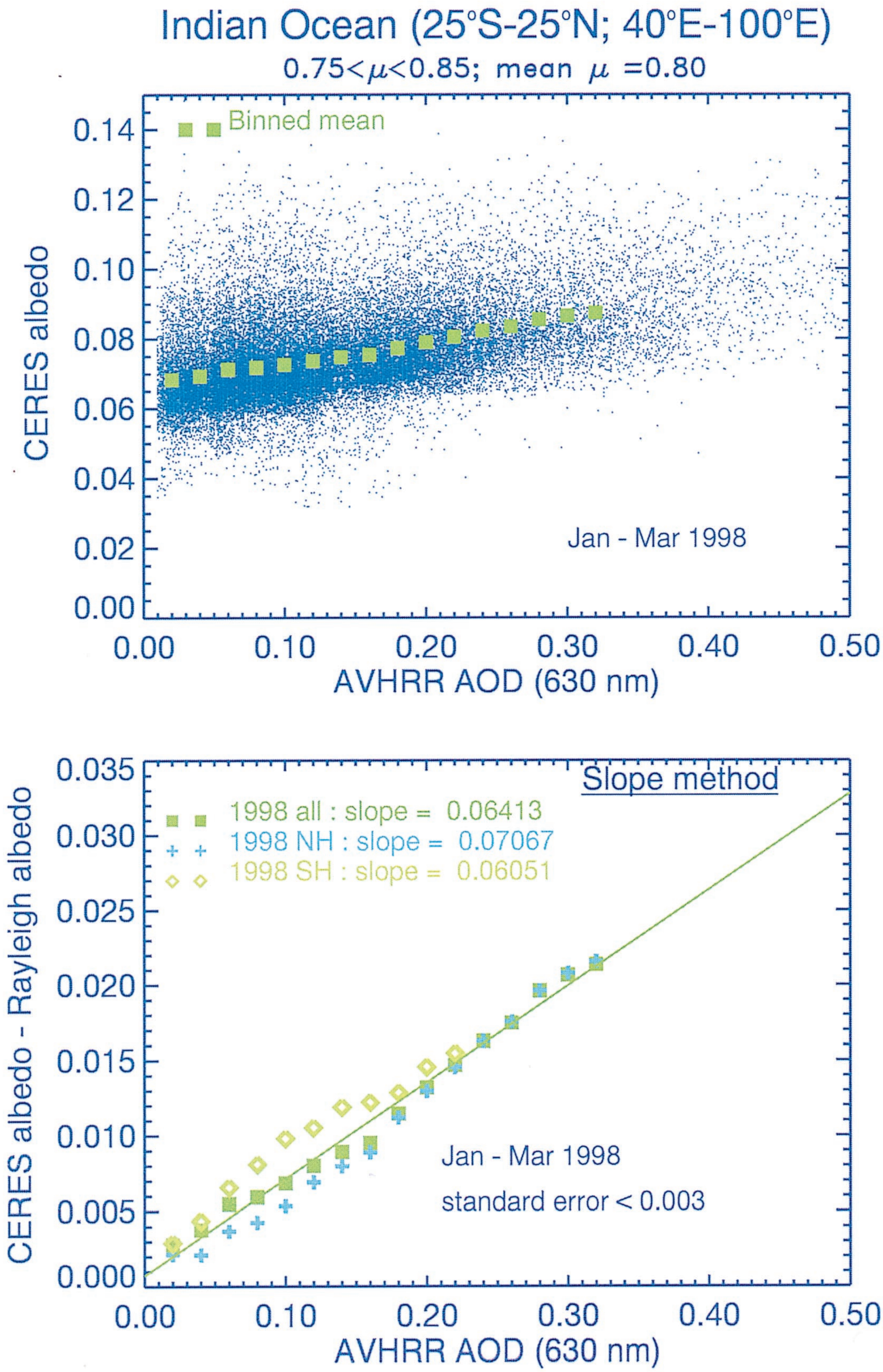

Plate 1. (top) Scatterplot of the observed clear-sky TOA albedo and the corresponding collocated AOD over the Indian Ocean during the period January 1 to March 31, 1998 (with μ in the range of 0.75-0.85). The mean TOA albedos for each AOD interval of 0.02 are indicated using solid square symbols. (bottom) Variation of the aerosol contribution to TOA albedo with AOD. Only the mean values are shown. The variations for Northern and Southern Hemisphere Indian Ocean also are shown.

erties observed over the Indian Ocean island of Kaashidhoo (4.97°N, 73.466°E) into a Monte Carlo radiative transfer model, *Podgorny et al.* [2000] showed that during the winter period, aerosols decrease the sea surface clear sky solar heating by about 16 W m^{-2}. The corresponding estimated direct radiative forcing at the top of the atmosphere (TOA) was about -4 Wm^{-2}. *Satheesh and Ramanathan* [2000] have estimated the clear sky aerosol forcing over Kaashidhoo based on observations during the winter period of 1998 and 1999 which showed that the diurnal mean clear sky solar flux decreased at the surface by 15–30 Wm^{-2}, while at TOA it increased only by 5–10 Wm^{-2}, the balance being distributed in the atmosphere.

The aerosol optical depth (AOD) derived using the advanced very high resolution radiometer (AVHRR) data over the ocean areas around the Indian subcontinent and the TOA broadband short wave (SW) radiative flux observed using the Clouds and the Earth's Radiant Energy System (CERES) [*Wielicki et al.*, 1996] at the same location and time provide a unique opportunity to estimate the clear sky radiative forcing due to aerosols in the Earth-atmosphere system over the entire Indian Ocean region. The primary objectives of the present study are (1) the estimation of the clear sky aerosol radiative forcing efficiency (i.e., the change in the clear sky SW radiative flux with unit increase in AOD) at the TOA and (2) the determination of the regional clear sky aerosol radiative forcing at the TOA and surface and studying its interannual variability during the Asian winter monsoon period (January-March) over the tropical Indian Ocean, Arabian Sea, and Bay of Bengal. The study is based on the AOD at 630 nm retrieved from the channel 1 (630 ± 50 nm) radiance observed by AVHRR on onboard NOAA 14 [*Rajeev et al.*, 2000] and TOA broadband SW radiative flux (in the spectral range of 0.3 μm-5.0 μm) observed using CERES [*Wielicki et al.*, 1996] over the region during the winter monsoon period of January-March 1997, 1998, and 1999. The satellite retrieval model for deriving AOD from NOAA 14 AVHRR data is based on the observed chemical and optical properties of aerosols over the Indian Ocean, the in situ measured value of single-scattering albedo, and the wind dependence of sea surface reflectance [*Rajeev et al.*, 2000]. The aerosol forcing efficiency is estimated using the collocated values of AVHRR-retrieved AOD and the TOA albedo observed using CERES during January 1 to March 31, 1998, and March 1–31, 1999. Regional maps of TOA aerosol forcing during January-March 1997, 1998, and 1999 are then generated using the AVHRR retrieved AOD and the estimated clear sky aerosol forcing efficiency. Using the observed regional clear sky aerosol forcing at TOA and the ratio of the surface to TOA clear sky aerosol radiative forcing observed over the Indian Ocean island of Kaashidhoo based on in situ measurements reported by *Satheesh and Ramanathan* [2000], regional maps of the clear-sky aerosol radiative forcing at the surface and within the atmosphere are generated (for a region within ±10° around Kaashidhoo), and its interannual variability is discussed.

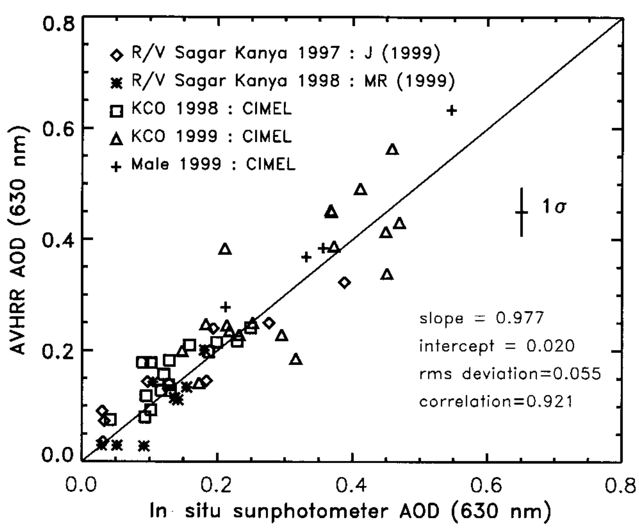

Figure 1. Intercomparison of the advanced very high resolution radiometer (AVHRR) aerosol optical depth (AOD) with the in situ AOD. The in situ measurements were obtained from the automatic CIMEL Sun/sky radiometer at the Kaashidhoo Climate Observatory (KCO) (4.96°N, 73.46°E) and Male' (4.19°N, 73.52°E), the hand-held Sun photometer onboard R/V *Sagar Kanya* during 1997, and the spectroradiometer onboard R/V *Sagar Kanya* during 1998.

2. Data and Method of Analysis

2.1. Retrieval of Aerosol Optical Depth From NOAA 14 AVHRR Data

The AOD (at the wavelength 630 nm ± 50 nm) over the Indian Ocean area (in the latitude range 25°S to 25°N and the longitude range 40°E-100°E) during January 1 to March 31 of 1997, 1998, and 1999 is retrieved from the radiance observed by channel 1 of NOAA 14 AVHRR. The methodology is explained by *Rajeev et al.* [2000]. We have used the NOAA 14 AVHRR global area coverage (GAC) data of the afternoon satellite pass. Revised postlaunch calibration constants which correct for the degradation of the AVHRR channel 1 sensor are used to convert the AVHRR digital counts to reflectance [*Rao and Chen*, 1999]. Retrieval of AOD is based on comparison of the observed satellite radiance at channel 1 with the look-up tables of modeled radiances. The look-up tables of satellite radiances as a function of solar zenith angle, the satellite viewing angle, relative azimuth, surface wind speed, and AOD are generated using the discrete ordinate radiative transfer method for a plane parallel atmosphere [*Stamnes et al.*, 1988] with 32 vertical layers. This method accounts for the multiple scattering by aerosols and molecules and absorption due to aerosols, water vapor, and ozone. Vertical profiles of pressure, temperature, molecular density, and ozone for the tropical atmosphere are based on the model by *McClatchey et al.* [1972]. Aerosols are assumed to be well mixed in the boundary layer (up to 1 km), and the aerosol number density decreases exponentially with height above 1 km with a scale height of 0.8 km, which is inferred from the lidar images during the observation period [*Satheesh et al.*, 1999]. To minimize errors in the retrieval of AOD, we use the data only from the antisolar side of the satellite scan. Variations in ocean reflectance due to wind speed are taken into account by considering daily surface winds from the National Centers for Environmental Prediction (NCEP) and the National Center for Atmospheric Research (NCAR) reanalysis [*Kalnay et al.*, 1996]. Fresnel reflection of the direct and diffuse solar radiation at the ocean surface is calculated for rough ocean based on the model proposed by *Cox and Munk* [1954]. Increase in ocean albedo due to foam (whitecaps) with increase in wind speed is calculated on the basis of the model produced by *Kopke* [1984]. Pixels, which are filled partially or fully by clouds, are detected and rejected using three tests: (1) the threshold method (brightness temperatures in channels 4 and 5), (2) the spatial coherence test (brightness temperatures in channel 4) [*Coakley and Bretherton*, 1982], and (3) the visible and near-IR channel ratio method [*Durkee et al.*, 1991].

The aerosol scattering phase function and single-scattering albedo used in the retrieval are based on the aerosol model developed using observations of the chemical, microphysical, and optical properties of aerosols over the Indian Ocean during the winter months [*Satheesh et al.*, 1999]. This aerosol model contains seven aerosol types, namely, sea salt, sulfate, nitrate, organics, ammonia, dust, and soot. The aerosol scattering phase function used here is the same as that shown in Figure 1 of *Rajeev et al.* [2000]. The observed mean single scattering albedo at the surface is 0.90 and corresponds to a mean relative humidity of 78% observed during the period. However, the mean relative humidity varies with height, which results in the height variation of single scattering albedo. For the above described aerosol model, the values of aerosol single scattering albedo (ω) with relative humidity (RH) obtained on the basis of the *Hess et al.* [1998] model are 0.90 for RH = 78%, 0.874 for RH = 70%, 0.861 for RH = 60%, 0.850 for RH = 50%, and 0.752 for RH=35%. We have taken the average altitude profile of RH on the basis of the balloon sonde data during the observation period as given by *Satheesh et al.* [1999] and used the corresponding altitude variation of ω. The altitude profile of RH has a mean value of 78% in the mixing region (up to 1 km) and decreases above 1 km to have a mean value of 62% between 1 and 2 km. Above 2 km, RH shows only little variation and has a mean value of 35%. For this altitude variation of RH and corresponding variation in ω, the column integrated value of ω is 0.87 (with ω = 0.90 at the surface).

The in situ measured single scattering albedo at Kaashidhoo was ~0.9 at the surface. However, aerosols of purely oceanic origin have single-scattering albedo of ~1.0. Background AOD due to aerosols of ocean origin is, however, small (~0.05). Thus the application of the absorbing aerosol model with ω = 0.87 over the whole area and all optical depths may not be valid. For each clear sky pixel we retrieve two values of AOD, one using the absorbing model described above (with ω = 0.90 at the surface) and the other with ω = 1.0. The AODs retrieved using these two models were used to obtain the AOD used in this study as follows: If AOD retrieved using ω equal to 1.0 at a pixel is ≤0.05, this is taken as the actual AOD at the pixel. When AOD retrieved using the absorbing model at a pixel is >0.15, this value is taken as the AOD at the pixel. For values of AOD between 0.05 and 0.15, the AOD at the pixel is obtained by interpolating between the retrieved AODs using the absorbing model and that obtained using ω equal to 1.0, after assuming a nonabsorbing AOD of 0.05. Thus for higher AOD the value will be closer to that obtained using the obsorbing model. This accounts for the nonabsorbing background aerosols of marine origin (ω = 1.0) and continental aerosols which are observed to have single scattering albedo of 0.87 (0.9 at the surface). The AOD retrieved for each satellite pass is gridded horizontally with latitude-longitude grid size of 0.2° by averaging the AOD derived from all the clear sky individual pixels within the grid box.

The satellite-retrieved AOD is compared with the in situ measured AOD as shown in Figure 1. The in situ measurements were obtained from different sources. First is the automatic CIMEL Sun/sky radiometer, which is part of the Aerosol Robot Network (AERONET) [*Holben et al.*, 1998] at the Kaashidhoo Climate Observatory (KCO) (4.96°N, 73.46°E) and Male (4.19°N, 73.52°E) (interpolated to 630 nm using observations at 500 and 670 nm) during February 24, 1998, to March 31, 1998, and January 1 to March 31, 1999. The shipborne measurements during 1997 are based on a hand-held Sun photometer onboard R/V *Sagar Kanya* [*Jayaraman*, 1999] cruising between latitudes of 13°N and 13°S during January 1–31, 1997 (interpolated to 630 nm using observations at 497 and 667 nm). The shipborne measurements during 1998 were done using the spectroradiometer [*Meywerk and Ramanathan*, 1999] at 630 nm onboard R/V *Sagar Kanya* cruising between latitudes of 20°S and 20°N during February 18 to March 31, 1998. For comparison of satellite retrieved AOD with the Kaashidhoo data, we consider average AVHHRR AOD within ± 1.0° latitude-longitude and within a time interval of ±60 min. For comparison with the shipborne measurements, AVHRR AOD within ±2° latitude-longitude and within a time interval of ±60 min is considered. Restricting the horizontal extent of the AVHRR data to smaller horizontal ranges reduces the number of data points available for the intercomparison but the results are similar. The slope of the intercomparison shown in Figure 1 is 0.977 and the intercept is 0.020. The correlation coefficient is 0.921. The root-mean-square (RMS) deviation between the AVHRR and the in situ AOD is 0.055. Part of the spread in the intercomparison between the AVHRR AOD and the in situ measured value could be due to the spatial averaging of AVHRR AOD used in the intercomparison. On the basis of the sensitivity analysis discussed below and the intercomparison of AVHRR AOD with the in situ measured AOD, the typical uncertainty of the AVHRR derived AOD is ~15%.

The satellite-derived AOD is sensitive to the aerosol phase function; the single scattering albedo, the surface reflectance, and the AVHRR calibration constants used in the retrieval. The sensitivity of the above parameters on the satellite derived AOD are discussed here. The sensitivity of the derived AOD to surface reflectivity and aerosol single scattering albedo is shown by *Rajeev et al.* [2000]. Figure 2 shows sensitivity of the derived AOD to the aerosol single scattering albedo (ω), which is found to be the largest source of uncertainty. All the satellite passes during January 1999 are analyzed using the present method explained above with the aerosol model having ω = 0.87 (nonconservative scattering case) and ω = 1.0 (conservative scattering case), keeping all other parameters (including the phase function) the same, in order to study the effect of singlescattering albedo alone. In Table 1, case 1 shows the slope, intercept, and correlation of a linear fit to the two observations shown in Figure 2. It may be noted from Figure 2 that for high values of AOD the conservative scattering case underestimates the AOD by as much as 25-30% compared to the nonconservative scattering case. The difference is insignificant at very low AOD (<0.15). The agreement for low AOD values is an artefact, since our model assumes a purely nonabsorbing model for AOD ≤ 0.05 and a linear interpolation between ω = 1 and ω = 0.87 for AOD from 0.05 to 0.15. Over the Indian Ocean north of the Intertropical Convergence Zone (ITCZ), ω = 0.87 is consistent with the surface, aircraft, and shipborne measurements conducted during January-March 1998 and 1999. South of the ITCZ, the AOD derived was generally low and hence the effective single-scattering albedo used by the model is more than 0.87 (mostly closer to 1.0), which is consistent with the above in situ measurements during

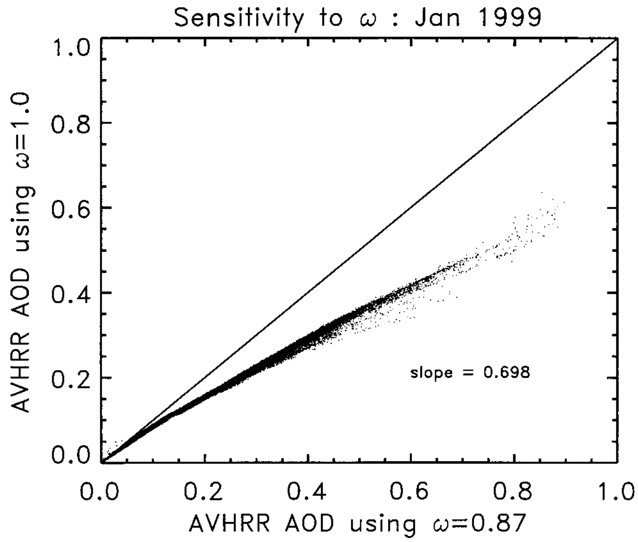

Figure 2. Sensitivity of the AVHRR AOD to the aerosol single-scattering albedo (ω) assumed in the retrieval. All the satellite passes during January 1999 are analyzed using the present method with the aerosol model having $\omega = 0.87$ and $\omega = 1.0$, keeping all other parameters (including the phase function) the same.

the period. This further justifies the methodology used in the present study by assuming that $\omega \approx 1.0$ at low AOD values and $\omega_a = 0.87$ only at AOD > 0.15. Table 1 also shows the correlation between the AOD derived with different parameters to study the effect of the parameters such as the aerosol phase function, surface reflectance, and AVHRR calibration constants, keeping all other parameters the same. The method used is the same as that described above, and the slope, intercept, and correlation coefficients are obtained by the correlation of the results of the analysis of 31 days of all satellite passes during January 1999 for the entire region of study presented here by varying the stated parameters. As seen for case 2 in Table 1, the AOD derived using the present model is ~14% less compared to the marine tropical aerosol model of *Hess et al.* [1998] as seen from the value of slope, while the offset in this case is very close to zero. The AVHRR calibration constants of *Rao and Chen* [1999] and that of *Tahnk and Coakley* [2001] are consistent and did not have any significant effect on the derived AOD, since the slope is close to unity and the offset is close to zero (case 3). In case 4 (to study the effect of surface reflectance assumed in the satellite retrieval) the slope is close to unity, while the offset is 0.027. This means that the effect of assuming a constant surface reflectance, as against a wind-dependent albedo, is mainly to shift the derived AOD by a nearly constant value.

2.2. Clear-Sky TOA SW Radiation Flux and Albedo Observed by CERES

CERES is part of the NASA Earth Observing System (EOS) and provides a continuation of the Earth Radiation Budget Experiment (ERBE) record of radiation fluxes at TOA. CERES data are analyzed using the same technique as the existing ERBE data [*Wielicki et al.*, 1998]. The accuracy of CERES data is considered to be better than the existing ERBE data. The data used here were obtained from CERES onboard the Tropical Rainfall Measuring Mission (TRMM) launched on November 1997. TRMM is a 35° inclined, precessing orbit satellite which provides higher temporal coverage (but limited to the tropics) compared to the historical ERBE product obtained from both the Sun-synchronous satellites and the low inclination precessing orbit. Pixel resolution of CERES onboard TRMM is 10 km at nadir, which enables it to observe more clear sky area compared to the conventional ERBE data with 40 km resolution. CERES observes the radiance in three spectral bands: (1) the total spectral band (0.3–200 μm), (2) the thermal spectral band (5–200 μm), and (3) the window region (8–12 μm). The broadband shortwave radiance (in the wavelength range of 0.3–5 μm) is obtained by subtracting the observed radiance in the thermal band from that in the total band and is converted to unfiltered SW radiance based on the instrument spectral characteristics. The SW radiance is converted to TOA SW flux using the ERBE-like inversion [*Smith et al.*, 1986]. This set of processed CERES data is referred to as ERBE-like science (ES-8) data, and it contains the instantaneous SW radiative fluxes at TOA for each CERES field of view (FOV). We have used the edition 2 of CERES ES-8 data in this study. These ERBE-like TOA fluxes provide the most consistent data product with historical ERBE measurements. The TOA SW fluxes are converted to TOA albedos by dividing by the instantaneous incident solar flux at the geographic location. In the present study we have used only the pixels identified as "cloud free ocean." The error in the monthly mean pixel albedos is a few percent, while the uncertainty in the instantaneous values is about 12% [*Wielicki et al.*, 1998].

2.3. Collocating the AOD and SW Flux

There is at least one observation of TOA radiance by CERES over any given tropical location during 24 hours. However, because of the precessing nature of the TRMM orbit, the time of this observation varies from day to day. We stored the daily TOA clear-sky albedo for the region of 25°N to 25°S and

Table 1. Sensitivity of Aerosol Optical Depth to the Various Parameters Assumed in the Aerosol Retrieval

Case	*x* Parameter	*y* Parameter	Slope	Intercept	Correlation
1	$\omega_c = 0.87$	$\omega_c = 1.0$	0.698	0.013	0.996
2	present aerosol model but for $\omega_c = 1.0$	marine tropical model [*Hess et al.*, 1998] with $\omega_c = 1.0$	1.137	−0.012	0.979
3	AVHRR calibration by *Rao and Chen* [1999]	AVHRR calibration by *Tahnk and Coakley* [2001]	1.017	0.0040	0.999
4	wind-dependent surface reflectance	constant surface reflectance of 0.007	0.983	−0.027	0.992

40°E to 100°E for each 0.2° × 0.2° latitude-longitude grid box with a time resolution of 1 hour. The TOA latitude and longitude as given in CERES ES-8 data were converted to their surface values using the standard geometrical algorithm. Similarly, the mean AOD data for each day at any geographic location over the above region are stored with 0.2° latitude-longitude resolution. Unlike the TOA albedo obtained from the CERES data, the time of observation of AOD using AVHRR data is nearly constant (~1430 during January-March 1998). For each of the geographic cells of grid size 0.2° the AOD values are collocated with TOA albedo within a time interval of 2 hours, for each day. However, the precessing nature of the TRMM orbit and the higher frequency of occurrence of cloud over the tropics limit the number of data points that are thus collocated. The study is made with values of collocated CERES broadband TOA albedo and the AVHRR AOD during the period January 1 to March 31, 1998, when a sufficient number of collocated data points were available over the region. During 1999, the CERES data were available only during March (not continuous) due to operational problems with the satellite, and the number of collocated data points available is too low compared to 1998. Hence the CERES data during 1999 are used here only for assessing the validity of the results obtained for the 1998 period.

3. Model Computations of TOA Flux

To determine the clear sky aerosol radiative forcing from the collocated AOD and TOA albedo, the molecular contribution has to be subtracted from the observed TOA albedo (in the slope method discussed in section 4.1). In the present study, the molecular contribution to the TOA albedo for various solar zenith angles is determined using the Monte Carlo model described by *Podgorny et al.* [2000]. In this broadband model, the entire solar spectrum is divided into 38 spectral bands and has 33 vertical layers between the surface and 100 km. The ocean surface albedo to direct solar radiation is based on the model by *Briegleb et al.* [1986]. The ocean albedo for diffuse downward radiation is taken as 6.0% as suggested by *Briegleb et al.* [1986]. These model computations were also performed with aerosols present in the atmosphere. The aerosol model properties used (the single scattering albedo and its altitude variation, the aerosol scattering phase function, and altitude variation of aerosol extinction) are the same as that explained in the aerosol model described in section 2.1.

4. Results and Discussion

4.1. Estimation of Clear-Sky Aerosol Radiative Forcing Efficiency at TOA

The clear sky aerosol forcing efficiency at TOA is estimated on the basis of two independent methods: (1) the slope method and (2) the differencing method. The slope method is limited to a finite range of μ (=cos(θ), where θ is the solar zenith angle) due to the unavailability of a sufficiently large number of data points for all ranges of μ. This is a potential limitation of this method since the aerosol forcing is a function of the solar zenith angle. The differencing method, on the other hand, uses all observed values of μ and accounts for the dependence of aerosol forcing on μ.

4.1.1. Slope method. Plate 1 (top) shows the scatterplot of the observed clear-sky TOA albedo and the corresponding collocated AOD over the geographic area between 25°N and 25°S and between 40°E and 100°E for the period January 1 to March 31, 1998. Since the TOA albedo depends strongly on the solar zenith angle, we include only values within a narrow range of μ between 0.75 and 0.85. The particular range was chosen because it had the maximum number of collocated data points. The mean value of μ is 0.80. The total number of collocated data points is 37,709. The mean TOA albedos for each AOD interval of 0.02 are indicated using solid square symbols, which are indicated only for the range of AOD values having at least 200 points within the 0.02 range of AOD. The standard deviation of the TOA albedo for any given AOD is in the range of 12-16%. The relatively large scatter in the values is due to the uncertainties in the model used to convert radiances to TOA albedo (the standard deviation due to this factor alone is about 12.1% as described in section 2.2) and due to cloud contamination. The uncertainties in the retrieved AOD (typically 15%) and the variation in the TOA albedo with solar zenith angle ($0.75 < \mu < 0.85$) also contribute to this scatter. Despite the relatively large scatter in the values, the increase in TOA albedo with AOD is clearly discernible in the top plot of Plate 1. The slope of the variation of the mean TOA albedo (binned at AOD intervals of 0.02) is 0.0646 and the intercept is 0.0664. The intercept represents the value of clear sky albedo in the absence of aerosols, i.e., due to reflection by surface and scattering by air molecules. In principle, the slope is the aerosol forcing efficiency. However, to establish its validity, we estimate it more directly in the bottom plot of plate 1, after subtracting the aerosol-free TOA albedo for each individual observation.

The aerosol-free TOA albedo is based on the Monte Carlo model estimations of *Podgorny et al.* [2000] as discussed in section 3. The difference between the observed TOA albedo (top plot of Plate 1) and the aerosol-free TOA albedo based on the model calculations gives the TOA albedo due to aerosols alone (α_a). The individual α_a values thus determined are then averaged at AOD intervals of 0.02 to obtain the mean α_a and are shown in the bottom plot of Plate 1; they are indicated only for the range of AOD values having at least 200 points within the 0.02 range of AOD. The standard deviation of the individual mean α_a values is the same as that of the mean albedo values in Plate 1 (top). The standard error (standard deviation divided by the square root of the number of values in each AOD bin) of the mean α_a values is less than 0.003. The bottom plot of Plate 1 shows a very nearly linear increase in α_a with AOD, and the variation is appreciably higher than the individual standard errors. The slope of the straight line obtained by a least squares fit is 0.0646, which gives the clear-sky aerosol radiative forcing efficiency at TOA for $\mu = 0.80$. This value is in good agreement with the slope in Plate 1. (top). The intercept of the least square fitted line in Plate 1 (bottom) is very close to zero (0.0007). The near-zero intercept in the bottom plot demonstrates that the intercept in the top plot is an excellent approximation for the albedo of the aerosol-free atmosphere for a mean μ of 0.80. Furthermore it also validates the Monte Carlo model calculations.

Plate 1 (bottom) also shows the clear-sky aerosol forcing efficiency for the northern (north of the equator) and southern (south of the equator) Indian Ocean. The clear-sky aerosol forcing efficiencies. (i.e., the slope) for the northern and southern Indian Oceans are very similar and within the uncertainty limits. One of the main reasons for this is that the ITCZ is south of about 5°S to 10°S and the anthropogenic aerosols extend south of the equator. Hence the data for the entire

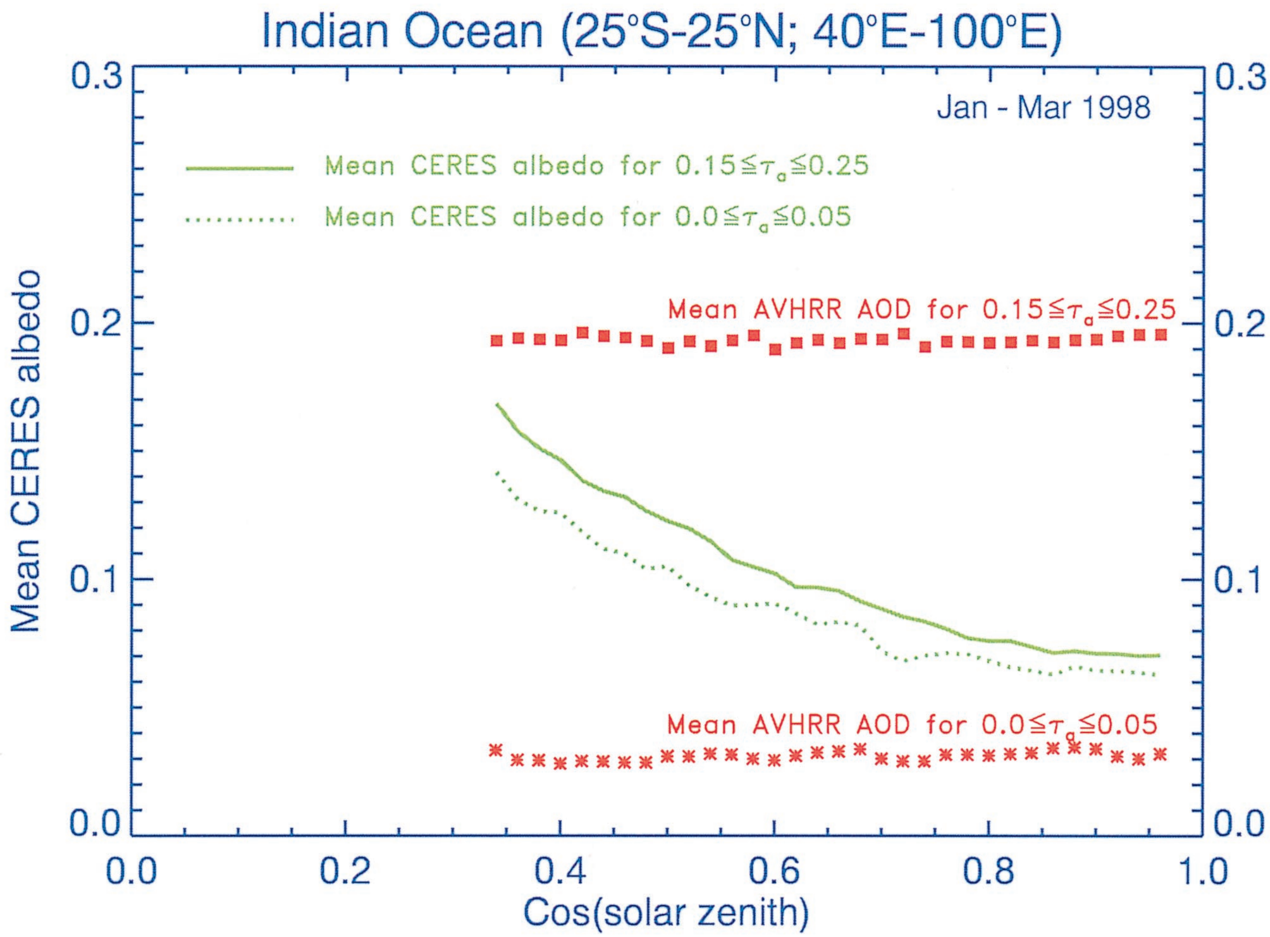

Plate 2. Variation of mean albedos (α_1 and α_2) with μ for two ranges of AOD ($0.0 \leq$ AOD ≤ 0.05 and $0.15 \leq$ AOD ≤ 0.25). The bin size of μ is 0.02. The respective mean AODs (τ_{a1} and τ_{a2}) are also shown. All the collocated data in the geographical area between 25°N and 25°S and between 40°E and 100°E during the period January 1 to March 31, 1998, are used here.

tropical Indian Ocean region are combined together, and the Northern Hemisphere and Southern Hemisphere are not treated separately for further calculations. As described in section 2.2, the maximum uncertainty in the TOA albedo is 12.1% and that in the AVHRR-retrieved AOD is ~15%. The two errors are not correlated. Thus the uncertainty in the aerosol forcing obtained on the basis of the above method is estimated to be less than 19.2%. The clear-sky aerosol radiative forcing efficiency at TOA (in terms of albedo and for AOD of 630 nm) is thus 0.0646 ± 0.0129 for $0.75 \leq \mu \leq 0.85$. The clear-sky aerosol forcing efficiency obtained from a similar analysis for the March 1999 (number of collocated points is only 7585) is 0.0496 for $0.75 \leq \mu \leq 0.85$. The results are in agreement within the uncertainty limits.

In the above computations, only the data with μ in the range $0.75 \leq \mu \leq 0.85$ are used, with a mean value $\mu_0 = 0.80$. The instantaneous clear-sky aerosol radiative forcing efficiency thus determined corresponds to $\mu_0 = 0.80$. We adopt the differencing method to extend the analysis to all zenith angle ranges. First, we ensure the consistency of the two approaches for $\mu = 0.80$.

4.1.2. Differencing method. The CERES TOA albedos are sorted for two ranges of collocated AOD: (1) $0.0 \leq$ AOD ≤ 0.05 and (2) $0.15 \leq$ AOD ≤ 0.25 and binning the mean albedo (α_1 and α_2 for $0.0 \leq$ AOD ≤ 0.05 and $0.15 \leq$ AOD ≤ 0.25, respectively) for each value of μ with bin size of 0.02. This method is applied only to the 1998 data. The number of points for most of the range bins of μ is insufficient during 1999 for the application of this method. Plate 2 shows the variation of mean albedos, α_1 and α_2 as a function of μ for the two ranges of AOD. The mean albedo increases with a decrease in μ, as would be expected from theoretical considerations. The corresponding mean AODs (τ_{a1} and τ_{a2}, respectively) are ~0.03 and 0.2, respectively, and uncorrelated with μ. It may be noted that the difference between the two mean albedos increases with a decrease in μ, which is an indication of the μ dependence of the clear-sky aerosol forcing efficiency.

The aerosol forcing efficiency for each interval of μ is determined by taking the ratio of the difference between α_1 and α_2 ($=\Delta\alpha$) to the corresponding difference between τ_{a1} and τ_{a2} ($=\Delta\tau_a$); that is, the clear-sky aerosol forcing efficiency as a function of μ is given by $f_e(\mu) = \Delta\alpha/\Delta\tau_a$. Variation of $f_e(\mu)$ as a function of μ thus calculated is shown in Figure 3 using solid square symbols. The value of f_e decreases with an increase in μ. The solid line shows the quadratic fitted to the observed forcing, given by $f_e(\mu) = a + b\mu + c\mu^2$, where $a = 0.\ 3259$, $b = -0.5684$, and $c = 0.2825$. The aerosol forcing based on the Monte Carlo model described in section 3 is also shown in

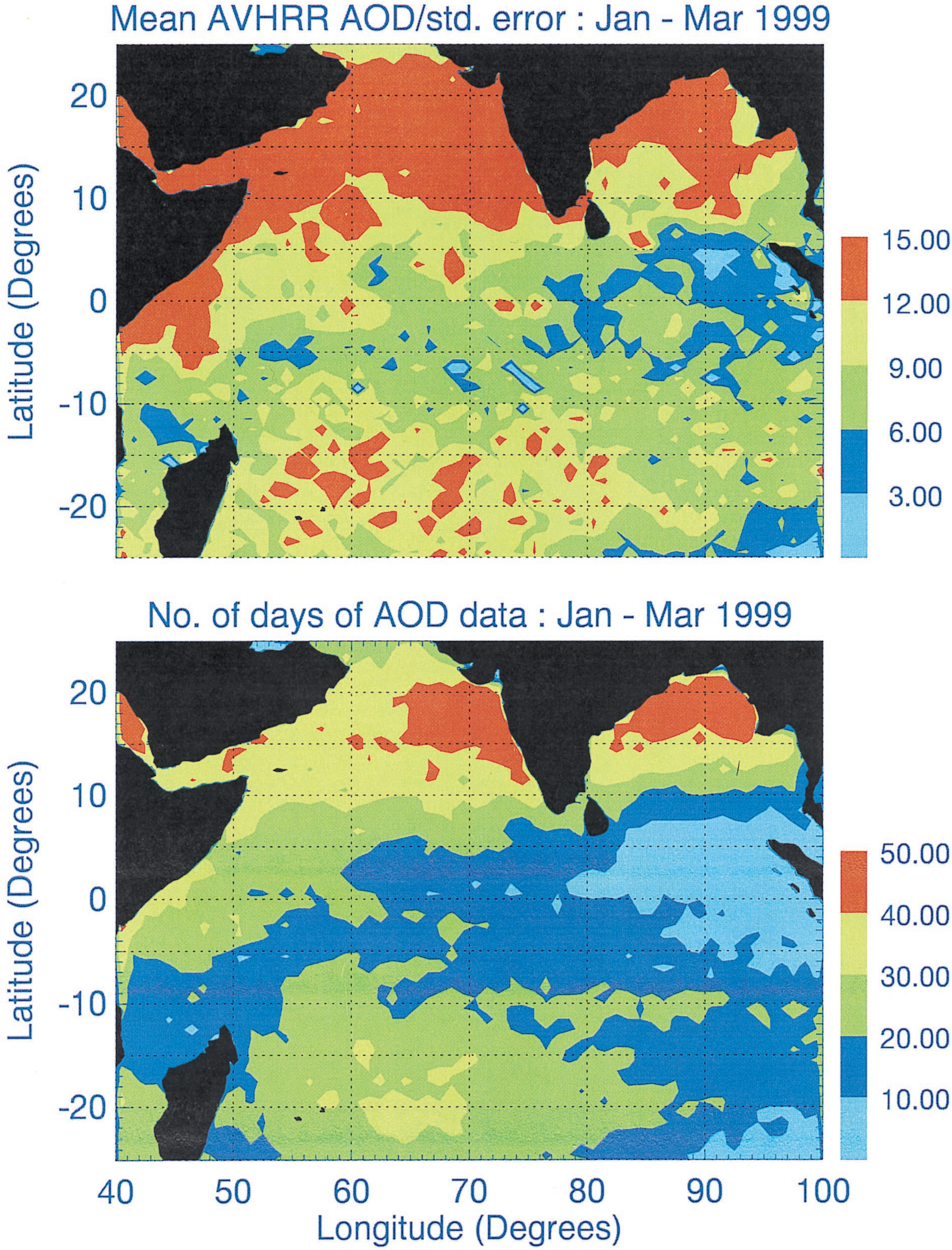

Plate 3. (top) Ratio of the seasonal mean AOD to the standard error (defined as the ratio of standard deviation to square root of the number of observations) during the period of January-March 1999. (bottom) Number of days of observation over the area of study during January-March 1999.

Figure 3 for comparison. The forcing efficiency obtained by the model shows very similar variation compared to the observed forcing but is slightly larger than the observed values.

The aerosol forcing efficiency at $\mu = 0.80$ using the quadratic fit to the observed forcing in this method is 0.0519, while that obtained using the differencing method is 0.0641, which is 19% more than the former, but within the uncertainty limit of the derived forcing efficiencies (~20%). Because the differ-

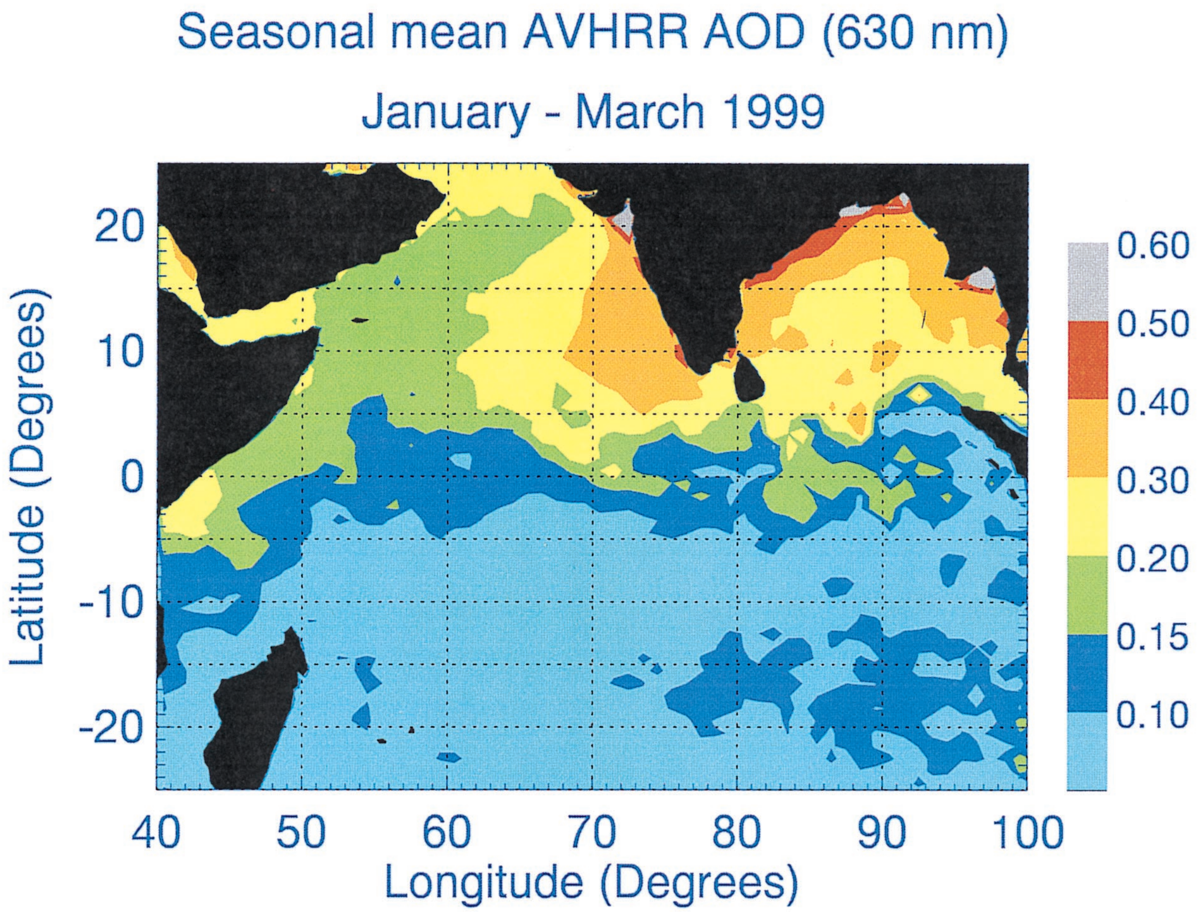

Plate 4. Seasonal mean aerosol distribution over the Indian Ocean during the period January-March 1999.

encing method gives the dependence of forcing efficiency as a function of μ, which is essential for the estimation of the diurnal mean forcing efficiency, and because the agreement between the slope method and the differencing method is within the limits of uncertainty, we have used the clear-sky aerosol forcing efficiency obtained using the differencing method in the subsequent calculations.

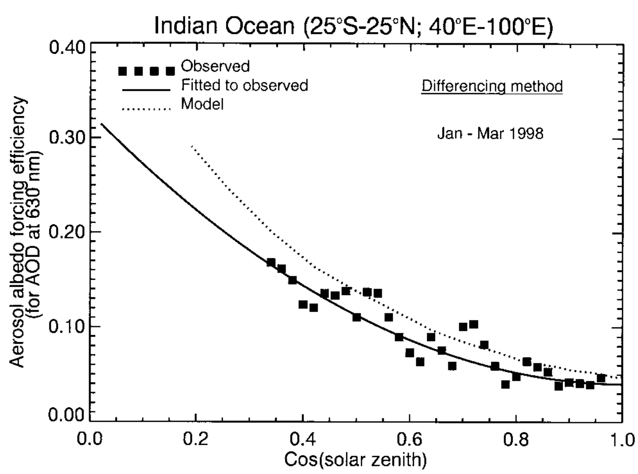

Figure 3. Variation of the observed clear-sky aerosol radiative forcing efficiency with μ (solid squares). The solid line shows the quadratic fitted to the observed forcing efficiency given by $f_e(\mu) = a + b\mu + c\mu^2$, where $a = 0.3259$, $b = -0.5684$, and $c = 0.2825$. The dotted line shows the aerosol forcing efficiency based on the Monte Carlo model.

4.2. Diurnal Mean Clear-Sky Aerosol Forcing Efficiency (f_d)

The diurnal mean clear-sky aerosol forcing efficiency on any given day is calculated by accounting for the instantaneous solar flux at any given geographic region and the μ-dependent clear-sky aerosol forcing efficiency discussed in section 4.1, using the relation

$$f_d = \frac{S_0}{2\pi}\left[\frac{d_0}{d}\right]^2 \int_{-h0}^{h0} cos(\theta) f_e(\theta) d\theta \qquad (1)$$

where S_0 (=1367 Wm^{-2}) is the mean solar flux per unit area at the mean Sun-Earth distance (d_0) for the perpendicular beam with $\theta = 0$, d is the Sun-Earth distance on the given day of the year, and h_o is the hour angle at sunrise and sunset. The value of $f_e(\theta)$ is obtained by the differencing method explained in section 4.1.

Figure 4 shows the diurnal mean clear-sky aerosol forcing efficiency, f_d, as a function of latitude and Julian day. Though in our calculations we have used the value of f_d at 630 nm

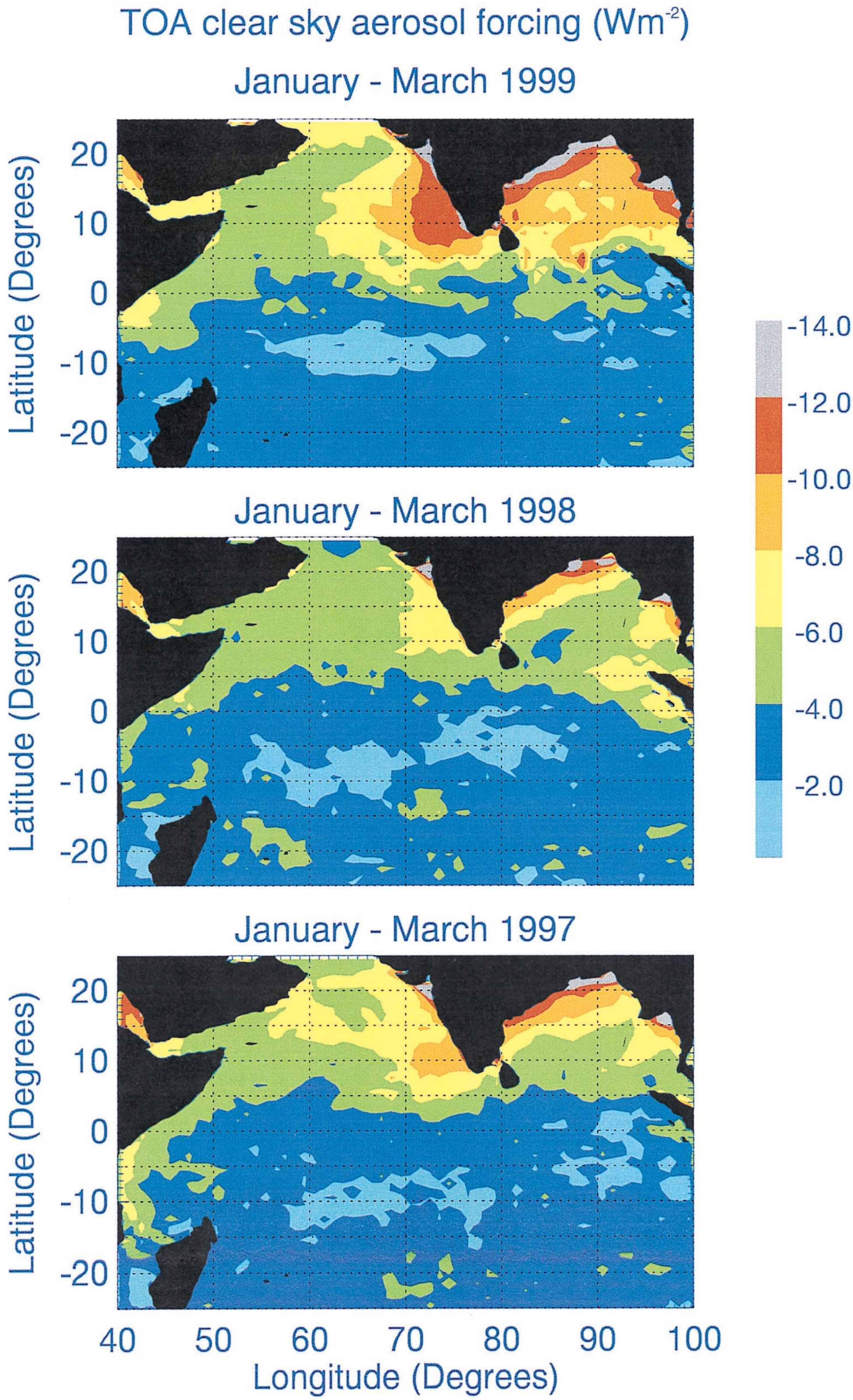

Plate 5. Regional maps of the observed clear-sky aerosol forcing at TOA during January-March 1997, 1998, and 1999.

which corresponds to the wavelength of the observed AVHRR AOD, the value at 500 nm is shown in Figure 4 for comparison with other measurements, most of which are made at 500 nm. The clear-sky aerosol forcing efficiency at 630 nm is converted to 500 nm by dividing by 1.30, which is the average ratio of aerosol optical depth at 500 nm to that at 630 nm based on the in situ measurements of AOD at KCO. The value of f_d is in the range of 23- 27 W m^{-2} (for unit increase in AOD at 500 nm), and on most of the latitudes and days of observation, f_d is close to 24 Wm^{-2}. The high value of f_d seen at the southernmost latitudes during January is because of the Sun's being in the Southern Hemisphere during this time, resulting in higher solar flux and increased duration of the daytime. The uncertainty of f_d is ~20%, i.e., about 5 Wm^{-2}.

4.3. Regional Distribution of Clear-Sky Aerosol Radiative Forcing at TOA

The clear-sky aerosol radiative forcing at TOA (F_t) is calculated by multiplying the observed AOD with the diurnal mean clear-sky aerosol forcing efficiency, f_d, obtained in section 4.2. Here we present the seasonal and diurnal mean clear-sky aerosol forcing during the period of January-March 1997, 1998, and 1999. For deriving the seasonal mean aerosol forcing, the data at a given location are averaged for the period of January to March of each year. However, the AOD has temporal variations and is also limited only to the clear-sky conditions. Representativeness of the data to generate the seasonal mean is thus affected by these two factors. The number of days of observation over the area of study during January-March 1999 is shown in Plate 3 (bottom). Since the aerosol retrieval is made only in the antisolar region of the satellite scan and the overlapping between successive satellite scans is insignificant at the low latitudes, the maximum number of days of observation is approximately half of the total number of days. Furthermore, within the ITCZ region, the probability of cloudiness is very large, which results in a significantly reduced number of days of observations in this region. The number of observations over the ITCZ around 85°E-100°E (the region close to Sumatra) is very low because of the very active convection in this region, particularly during 1999. Plate 3 also shows the ratio of the seasonal mean AOD to the standard error in AOD (defined as the ratio of the standard deviation of AOD to square root of the number of observations) during the period of January-March 1999 (top). The former may be considered as the signal and the latter as the noise. It may be noted that the signal-to-noise (S/N) ratio is sufficiently high (>6) over most of the regions of observation during the period except at the ITCZ. At the ITCZ the variability of AOD is higher. As seen later (e.g., Plate 4), the value of AOD is very small at ITCZ, which also contributes to the smaller signal-to-noise ratio. Considering the S/N ratio and the number of days of observation, we believe that the seasonal means derived are quite representative for most of the regions, except around the equator close to 85°E-100°E during 1999. The features are similar during 1997 and 1998. However, during 1997 and 1998 the number of observations at the equator close to 85°E-100°E also was significantly higher than that during 1999.

Plate 4 shows the seasonal mean aerosol distribution over the Indian Ocean for January-March 1999. In the Northern Hemisphere, AOD is very high close to the Indian subcontinent, southeast Asia, and Arabia. However, at the ITCZ and the Southern Hemisphere the AOD is small (less than 0.10). The spatial distributions are very similar to the TOA clear-sky aerosol forcing shown in Plate 5 and hence are not shown here for 1997 and 1998. The latitude variation of aerosol optical depth over the Arabian Sea sector (60°E-80°E) and the Bay of Bengal sector (80°E-100°E) for 1997, 1998, and 1999 is shown in Figure 5. The large latitudinal gradient, north of about 5°S,

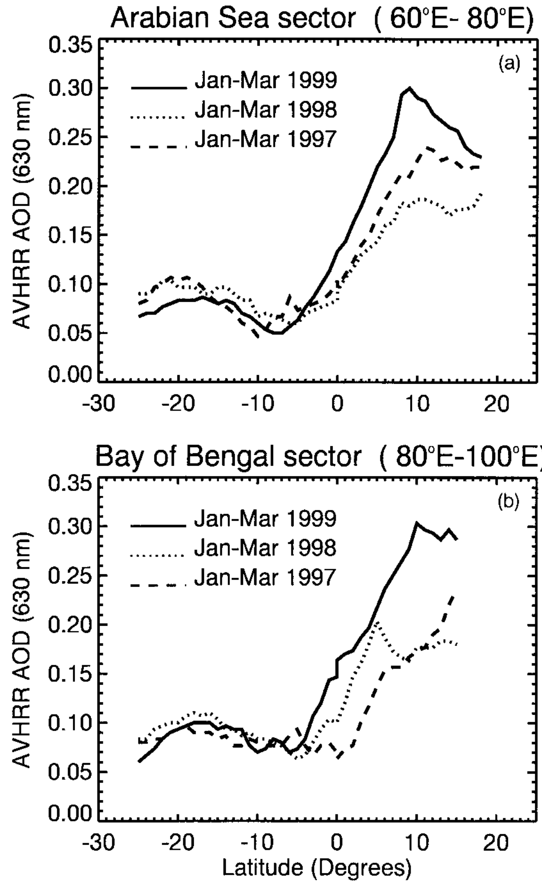

Figure 5. Latitude variation of the mean AOD at 630 nm over (top) the Arabian Sea sector (60°E-80°E) and (bottom) the Bay of Bengal sector (80°E-100°E) during January-March 1997, 1998, and 1999.

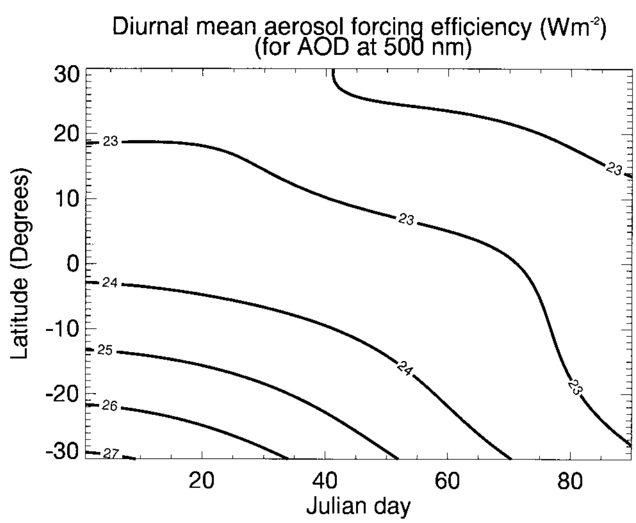

Figure 4. Diurnal mean clear-sky aerosol radiative forcing efficiency, f_d (for AOD at 500 nm) as a function of latitude and Julian day. The clear-sky aerosol forcing efficiency at 630 nm is converted to 500 nm by dividing by 1.30, which is the average ratio of aerosol optical depth at 500 nm to that at 630 nm obtained on the basis of the in situ measurements of AOD at the Kaashidhoo Climate Observatory (KCO).

is observed during all the years but with different magnitudes. The AOD during 1999 was the highest and that during 1998 was the lowest in the Northern Hemisphere. The features are very similar in both the Arabian Sea and the Bay of Bengal sectors.

Plate 5 shows the regional maps of the clear-sky aerosol forcing, F_t, during the winter monsoon period (January-March) of 1997, 1998, and 1999. The main features observed in Plate 5 are the following:

1. $|F_t|$ in the Northern Hemisphere (NH) is significantly higher than that in the Southern Hemisphere (SH) during all the three years of observation. The forcing is maximum close to the continents and decreases away from them.

2. $|F_t|$ is a minimum ($|IF_t|<3$ Wm^{-2}) close to the equator. This is the region of minimum AOD and is associated with the ITCZ. The large north-south gradient in F_t across the northern boundary of the ITCZ and in the Northern Hemisphere is remarkable over the all the longitudes.

3. $|F_t|$ slightly increases to the south of ITCZ in the SH and is associated with the increase in AOD. This increase in $|F_t|$ is approximately a factor of 1.2-1.5 compared to the minimum value observed at the ITCZ.

4. F_t shows considerable year-to-year variability in the NH. F_t is maximum in the NH during 1999 (in the range of -4 to -14 W m^{-2}) compared to the NH during 1997 and 1998. Near the Indian subcontinent and southeast Asia, F_t is in the range of -8 to -14 Wm^{-2} during 1999 and is a factor of 1.5–2 higher than the corresponding values during 1997 and 1998. These values may be compared with the seasonal (January-March) and diurnal mean incident solar flux, which is in the range of 455 Wm^{-2} (at 25°S) to 330 Wm^{-2} (at 25°N).

5. The year-to-year variability of F_t in the SH is significantly smaller than that in the NH. During the observation period the aerosol forcing in the SH is approximately the same during 1997, 1998, and 1999 and is mostly between 0 and -6 Wm^{-2}.

6. Though the overall year-to-year variation in the observed aerosol forcing is significant, the geographical pattern of the aerosol radiative forcing is strikingly similar during all three years of observation. High aerosol radiative forcing is observed over the south Arabian Sea close to the Indian subcontinent, northwest Bay of Bengal, southeast Asia, and Arabia. The minimum aerosol forcing in the ITCZ region and the increase in aerosol forcing around 15°S-25°S are observed during all three years of observation. The enhanced aerosol forcing observed during 1999 is mostly limited to the Northern Hemisphere and is almost completely absent in the Southern Hemisphere.

4.4. Latitude Variation of Clear-Sky Aerosol Radiative Forcing at TOA

The latitude variation of the seasonal mean (January-March) clear-sky aerosol radiative forcing at TOA is calculated by averaging F_t, over longitude ranges 50°-100°E and is shown in Figure 6 for 1997, 1998, and 1999. As may be seen in the latitude variation of AOD (Figure 5), the variations in the Bay of Bengal and the Arabian Sea are similar, and hence the regions are treated together in Figure 6. The overall trend in the latitude variation is similar during all three years of observation. The latitude gradient is highest north of about 5°S (the mean position of the ITCZ during the period). The difference between the aerosol forcing at 10°N and that at the ITCZ is ~4 W m^{-2} during 1997 and 1998, and approximately 7 Wm^{-2} during 1999. Between ITCZ and 25°S, the average radiative forcing is nearly the same during all three years of observation and is in the range -2 to -4 Wm^{-2}. There is a small increase (approximately -1 Wm^{-2}) in the aerosol forcing south of the ITCZ to reach a maximum value at ~18°S. The large latitude gradient in the clear-sky aerosol forcing can introduce a large gradient in the solar heating and may affect the circulation of the atmosphere. *Boucher at al.* [1998] suggested that during the Asian summer monsoon period, a large sulfate aerosol concentration over India and southeast Asia can weaken the pressure gradient over the Indian region and change large-scale circulation, which leads to a decrease in the rainfall over the region.

4.5. Clear-Sky Aerosol Radiative Forcing at the Surface

The presence of aerosols in the atmosphere changes the net solar radiation at the Earth's surface due to scattering and absorption. On the basis of the surface measurements of global, direct, and diffuse broadband radiation data, the TOA SW flux, and the in situ measurements of AOD at KCO, *Satheesh and Ramanathan* [2000] have shown that the ratio of surface to TOA clear-sky aerosol forcing is 3.0. This is close to the value of $R = 3.4$ given by *Podgorny et al.* [2000], using the Monte Carlo model incorporating the aerosol model developed over the Indian Ocean during the winter monsoon season. However, the model calculations also show that R varies with aerosol species and the single-scattering albedo. Thus the value of $R = 3.0$ may not be applicable over the entire Indian Ocean. Here we have estimated the aerosol radiative forcing at the surface from the TOA forcing assuming $R = 3.0$ as given by the direct observations of *Satheesh and Ramanathan* [2000], but limited to 5°S-15°N and 65°E-85°E, which is within approximately ±10° around KCO. Over this region, not far from Kaashidhoo, it is safe to assume that the value of R may not be significantly different from R=3.0 because (1) the aircraft and ship measurements conducted over the Indian Ocean during the Indian Ocean Experiment (INDOEX) by various groups [Ramanathan et al., 2001] suggest aerosol properties with single-scattering albedo similar to what is observed at Kaashidhoo, at least for regions north of 5°S, and (2) the study by *Jayaraman et al.* [1998] based on shipborne measurements has

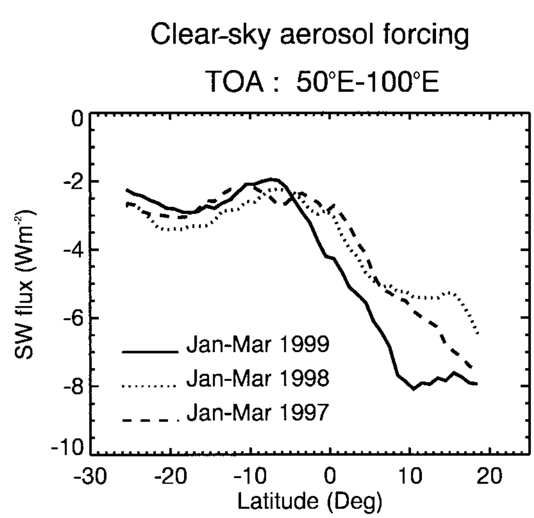

Figure 6. Latitude variation of the average seasonal mean (January-March) aerosol direct radiative forcing in the longitude ranges 50°-100°E during 1997, 1998, and 1999 at TOA.

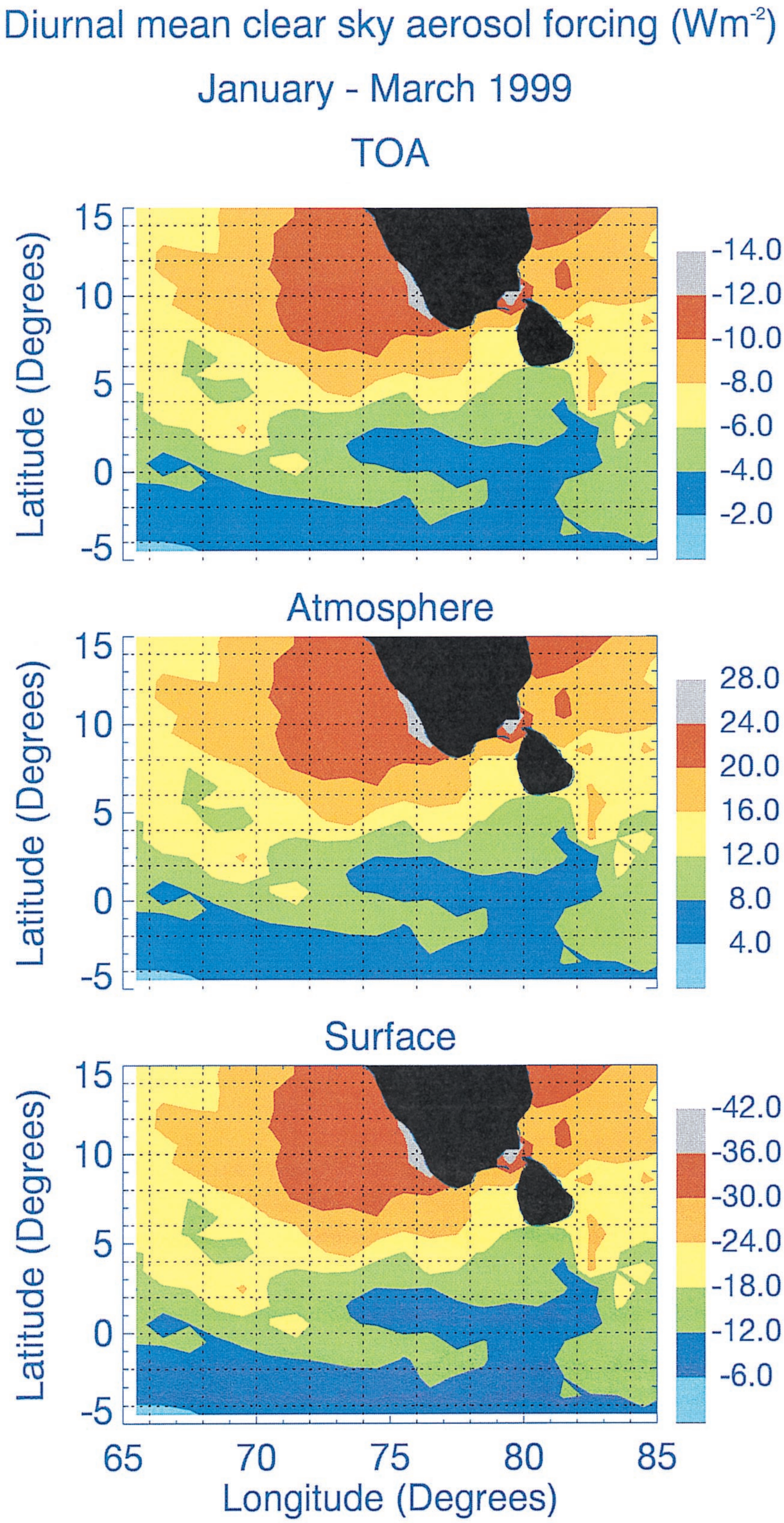

Plate 6. Clear-sky aerosol forcing at TOA, atmosphere, and surface during January-March 1999 over the region 65°-85°E and 5°S to 15°N.

shown similar aerosol forcing efficiencies over the study area north of about 5°S. The difference between the surface forcing and the TOA forcing is the net radiative heating of the atmosphere due to the presence of aerosols, in contrast to the cooling effect due to aerosols at the surface. Plate 6 shows the TOA, atmosphere, and surface clear-sky aerosol forcing during January-March 1999 over the region 65°-85°E and 5°S to 15°N. It may be noted that the magnitude (sign is negative) of the

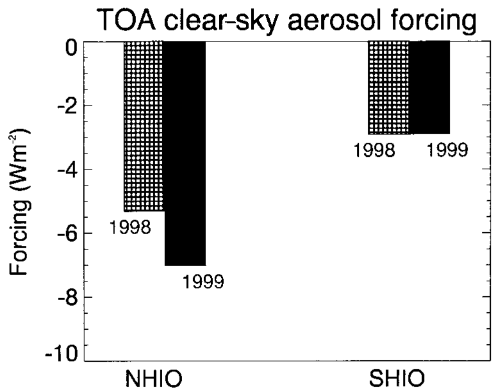

Figure 7. Comparison of the observed clear-sky aerosol, radiative forcing at the TOA in the Northern Hemisphere Indian Ocean (NHIO) and the Southern Hemisphere Indian Ocean (SHIO) during 1998 and 1999. The area encompassed between the equator and 25°N and between 50°E and 100°E is taken as the NHIO, and the area between the equator and 25°S and between 50°E and 100°E is taken as the SHIO.

aerosol forcing at the surface is greater than 18 Wm^{-2} over most of the regions in the NH, and about -30 to -42 Wm^{-2} close to the coastal boundary of the Indian subcontinent. Over Kaashidhoo, *Satheesh and Ramanathan* [2000] reported a value of approximately -22 and -33 Wm^{-2} during February and March 1999, respectively. This is in good agreement with -22.8 W m^{-2} over KCO during January-March 1999 estimated in the present study (the values of AOD and the aerosol forcing during January were less than those during February and March 1999). The atmospheric heating due to aerosols is estimated to correspond to ~12–28 Wm^{-2} over the NH and is ~20–28 Wm^{-2} near the coast of the Indian subcontinent.

Figure 7 shows the comparison of the observed clear-sky aerosol radiative forcing at TOA in the Northern Hemisphere Indian Ocean (NHIO) and the Southern Hemisphere Indian Ocean (SHIO) during 1998 and 1999. The area encompassed between the equator and 25°N and between 50°E and 100°E is taken as the NHIO, and the area between the equator and 25°S and between 50°E and 100°E is taken as the SHIO. Over the NHIO, observed aerosol forcing at the TOA is ~5.3 Wm^{-2} during 1998, while it is approximately -7.0 Wm^{-2} during 1999. The corresponding mean AODs at 630 nm during the period are 0.178 and 0.235 during 1998 and 1999, respectively. However, close to the continents the mean aerosol forcing is significantly higher. For example, over the Arabian Sea between 65°E and 75°E and between 5°N and 15°N, the mean aerosol forcing at TOA is -5.6 and -9.3 W m^{-2} during January-March 1998 and 1999, respectively. The TOA aerosol forcing is approximately -2.9 Wm^{-2} over the SHIO and is nearly the same during 1998 and 1999.

5. Conclusions

The study demonstrates that in situ and satellite data can be integrated to obtain the clear-sky aerosol forcing at TOA directly from observations. The collocated AVHRR AOD and CERES TOA SW flux data yield a TOA clear-sky aerosol forcing efficiency of about -24 Wm^{-2} (for AOD at 500 nm). Likewise, the KCO data of *Satheesh and Ramanathan* [2000] yield the ratio of surface to TOA forcing as 3.0. When the two results are employed with the AVHRR data, we obtain the regional map of the clear-sky aerosol forcing solely on the basis of observations. Thus the results presented here provide an initial data set to integrate on climate models for regional clear-sky aerosol radiative forcing. However, it is important to note that the present study is for clear-sky conditions only, and the AOD and clear-sky aerosol forcing presented here represent both the natural and the anthropogenic aerosols.

The study was restricted to the January-March (INDOEX period) 1997, 1998, and 1999. The principal findings of this study are as follows:

1. The clear-sky aerosol forcing efficiencies computed using two different methods are in excellent agreement. Their values are similar, at the Northern and Southern Indian Ocean, and during different periods of observations (1998 and 1999). The diurnal mean clear-sky aerosol forcing efficiency at TOA (i.e., the change in the diurnal mean flux at TOA for unit increase in AOD at 500 nm) is in the range of -23 to -27 Wm^{-2}, depending on the Julian day and latitude.
2. The clear-sky aerosol forcing is significantly larger in the Northern Hemisphere (-4 to -14 Wm^{-2} at TOA, -12 to -42 Wm^{-2} at the surface) compared to the Southern Hemisphere (0 to -6 Wm^{-2} at TOA) during the entire observation period. These values are substantially higher than the global mean values reported by *IPCC* [1995] for sulfate aerosols alone.
3. The TOA clear-sky aerosol forcing is minimum at the ITCZ region (0 to -3 Wm^{-2}), and its magnitude is higher by about 1.2 to 1.5 at the south of the ITCZ.
4. Both the AOD and the aerosol forcing show significant interannual variability in the Northern Hemisphere. Their values are highest during 1999, during which these values are higher than the corresponding values of 1997 and 1998 by a factor of $1.5 - 2.0$. The increase in aerosol loading observed during 1999 was highest close to the Indian subcontinent (both in the Arabian Sea and in the Bay of Bengal).
5. The interannual variations are almost insignificant in the Southern Hemisphere.
6. The latitude variations of AOD and the aerosol forcing are similar in the longitude sectors covering the Arabian Sea and the Bay of Bengal. The trend in the latitude variation of these parameters is similar during the three years of observation, though the magnitude of the latitude gradient is different, being highest during 1999 compared to 1997 and 1998.

The large clear-sky aerosol radiative forcing and its latitudinal gradient may alter the tropical temperature and pressure gradients, which in turn can affect the dynamics of the atmosphere. The Asian summer monsoon circulation is primarily driven by the north-south pressure gradient, and the effect of such large aerosol forcing on the summer monsoon should be studied using the circulation models. Further, the study needs to be extended to other seasons as well.

Acknowledgments. The CERES data were obtained from the NASA Langley Research Center EOSDIS Distributed Active Archive Center. We thank B. Barkstrom, B. A. Wielicki, and K. J. Priestley for switching on the CERES sensors during the INDOEX 1999 operations. The NCEP/NCAR reanalysis is provided by the NOAA-CIRES Climate Diagnostics Center, Boulder Colorado from their Web site at http://www.cdc.noaa.gov. The authors thank B. Holben for providing aerosol optical depth measurements at Male and Kaashidhoo Island in Maldives; the measurements are a part of AERONET. This study was funded by the National Science Foundation (NSF) through grant ATM 9612887. The Study was performed when one of the authors, K. R., was at the center for Clouds, Chemistry and Climate, Scripps Institution of Oceanography, University of California, San Diego.

References

Boucher, O., M. Pham, and R. Sadourny, General circulation model simulations of the Indian summer monsoon with increasing levels of sulphate aerosols, *Ann. Geophys., 16*, 346–352, 1998.

Briegleb, B. P., P. Minnis, V. Ramanathan, and E. Harrison, Comparison of regional clear-sky albedos inferred from satellite observations and model computations, *J. Clim. Appl. Meteorol., 25*, 214–226, 1986.

Charlson, R. J., S. E. Schwartz, J. M. Hales, R. D. Cess, J. A. Coakley, J. E. Hansen, and D. J. Hofmann, Climate forcing by anthropogenic aerosols, *Science, 255*, 423–430, 1992.

Coakley, J. A., and F. P. Bretherton, Cloud cover from high resolution scanner data: Detecting and allowing for partially filled fields of view, *J. Geophys. Res., 87*, 4917–4932, 1982.

Cox, C., and W. Munk, Measurement of the roughness of the sea surface from photographs of the Sun-glitter, *J. Opt. Soc. Am., 44*, 838–850, 1954.

Durkee, P. A., F. Pfeil, E. Frost, and R. Shema, Global analysis of aerosol particle characteristics, *Atmos. Environ., 25A*, 2457–2471, 1991.

Haywood, J. M., V. Ramaswamy, and B. J. Soden, Tropospheric aerosol climate forcing in clear-sky satellite observations over the oceans, *Science, 283*, 1299–1303, 1999.

Hess, M., P. Koepke, and I. Schult, Optical properties of aerosols and clouds: The software package OPAC, *Bull. Am. Meteorol. Soc., 79*, 831–844, 1998.

Hignett, P., J. P. Taylor, P. N. Francis, and N. D. Glew, Comparison of observed and modeled direct aerosol forcing during TARFOX, *J. Geophys. Res., 104*, 2279–2287, 1999.

Holben, B. N., T. F. Eck, I. Slutsker, D. Tanre, J. P. Buis, A. Setzer, E. Vermote, J. A. Reagan, Y. J. Kaufman, T. Nakajima, F. Lavenu, I. Jankowiak, and A. Smirnov, AERONET-A federated instrument network and data archive for aerosol characterization, *Remote Sens. Environ., 66*, 1–16, 1998.

Intergovernmental Panel on Climate Change (IPCC), *Climate Change, 1994: Radiative Forcing of Climate Change and Evaluation of IPCC IS92 Emission Scenarios*, edited by J. H. Houghton, 339 pp., Cambridge Univ. Press, New York, 1995.

Jayaraman, A., Results on direct radiative forcing of aerosols obtained over the tropical Indian Ocean, *Curr. Sci., 76*, 924–930, 1999.

Jayaraman, A., D. Lubin, S. Ramachandran, V. Ramanathan, E. Woodbridge, W. D. Collins, and K. S. Zalpuri, Direct observations of aerosol radiative forcing over the tropical Indian Ocean during the January-February 1996 pre-INDOEX cruise, *J. Geophys. Res., 103*, 13,827–13,836, 1998.

Kalnay, E. et al., The NCEP/NCAR reanalysis 40-year project, *Bull. Am. Meteorol. Soc., 77*, 437–471. 1996

Kaufman, Y. J., et al., Smoke, Clouds and Radiation-Brazil (SCAR-B) experiment, *J. Geophys. Res., 103*, 31,783–31,808, 1998.

Kiehl, J. T., and B. P. Briegleb, The relative roles of sulfate aerosol and greenhouse gases in climate forcing, *Science, 260*, 311–314, 1993.

Koepke, P., Effective reflectance of oceanic whitecaps, *Appl. Opt., 23*, 1816–1824, 1984.

McClatchey, R. A., R. W. Fenn, J. E. A. Selby, F. E. Volz, and J. S. Garing, Optical properties of the atmosphere, 3rd ed., *Environ. Res. Pap. 411*, Air Force Cambridge Res. Lab., Bedford, Masse, 1972.

Meywerk, J., and V. Ramanathan, Observations of the spectral clear-sky aerosol forcing over the tropical Indian Ocean, *J. Geophys. Res., 104*, 24,359–24,370, 1999.

Podgorny, I. A., W. Conant, V. Ramanathan, and S. K. Satheesh. Aerosol modulation of atmospheric and surface solar heating over the tropical Indian Ocean, *Tellus, Ser. B, 52*, 947–958, 2000.

Rajeev, K., V. Ramanathan, and J. Meywerk, Regional aerosol distribution and its long range transport over the Indian Ocean, *J. Geophys. Res., 105*, 2029–2043, 2000.

Ramanathan, V., et al., Indian Ocean Experiment (INDOEX) white paper, *Rep. C4*, Scripps Inst. of Oceanogr., Univ. of Calif., San Diego, La Jolla, Calif., Aug. 1995.

Ramanathan, V., et al., The Indian Ocean Experiment: An integrated analysis of the climate forcing and effects of the great Indo-Asian ocean haze, *J. Geophys. Res.*, in press, 2001.

Rao, C.R.N., and J. Chen, Revised post-launch calibration of the visible and near-infrared channels of the advanced very high resolution radiometer (AVHRR) on the NOAA-14 spacecraft, *Int. J. Remote Sens., 20(18)*, 3485–3491, 1999.

Russell, P. B, P. V. Hobbs, and L. L. Stowe, Aerosol properties and radiative effects in the United States East Coast haze plume: An overview of the Tropospheric Aerosol Radiative Forcing Observational Experiment (TARFOX), *J. Geophys. Res., 104*, 2213–2222, 1999.

Satheesh, S. K., and V. Ramanathan, Large difference in tropical aerosol forcing at the top of the atmosphere and Earth's surface *Nature, 405*, 60–63, 2000.

Satheesh, S. K., V. Ramanathan, X. Li-Jones, J. M. Lobert, I. A. Podgorny, J. M. Prospero, B. N. Holben, and N. G. Loeb., A model for the natural and anthropogenic aerosols over the tropical Indian Ocean derived from Indian Ocean Experiment data, *J. Geophys. Res., 104*, 27,421–27,440, 1999.

Smith, G. L., R. N. Green, E. Raschke, L. M. Avis, J. T. Suttles, B. A. Wielicki, and R. Davies, Inversion methods for satellite studies of the Earths radiation budget: Development of algorithms for the ERBE mission, *Rev. Geophys., 24*, 407–421, 1986.

Stamnes, K., S.-C. Tsay, W. Wiscombe, and K. Jayaweera, A numerically stable algorithm for discrete-ordinate-method radiative transfer in multiple scattering and emitting layered media, *Appl. Opt., 27*, 2502–2509, 1988.

Tahnk, W. R., and J. A. Coakley Jr., Improved calibration coefficients for NOAA-14 AVHRR visible and near-IR channels, *Int. J. Remote Sens.*, in press, 2001.

Wielicki, B. A., et al., Clouds and Earth's Radiant Energy System (CERES): An Earth Observing System Experiment, *Bull. Am. Meteorol. Soc., 77*, 853–868, 1996.

Wielicki, B. A., et al., Clouds and the Earth's Radiant Energy System (CERES): Algorithm overview, *IEEE Trans. Geosci. Remote Sens., 36*, 1127–1140, 1998.

K. Rajeev, Space Physics Laboratory, Vikram Sarathai Space Centre, Trivandrum 695 022, India. (krajeev@md5.vsnl.net.in)

V. Ramanathan, Center for Clouds, Chemistry, and Climate, Scripps Institution of Oceanography, University of California, San Diego, 9500 Gilman Drive, La Jolla, CA 92093. (vramanathan@ucsd.edu)

(Received April 26, 2000; revised October 6, 2000;
accepted October 11, 2000.)